Sputter Deposition of Aluminum Nitride for Applications in Thin-Film Resonators

by

Rajan Sharad Naik

BSc., Materials Science and Engineering
Cornell University, 1993

Submitted to the Department of Materials Science and Engineering
in partial fulfillment of the requirements for the degree of

Master of Science
in Materials Science and Engineering
at the
Massachusetts Institute of Technology
February 1996

© 1996 Massachusetts Institute of Technology. All rights reserved.

Signature of
Author...
Department of Materials Science and Engineering
January 19, 1996

Certified
by...
L. Rafael Reif
Director, Microsystems Technology Laboratories
Professor, Department of Electrical Engineering and Computer Science
Thesis Supervisor

Accepted
by...
Michael F. Rubner
TDK Professor of Materials Science and Engineering
Chair, Departmental Committee on Graduate Students

Read
by.......... ....
Eugene A. Fitzgerald
Professor, Department of Materials Science and Engineering

MASSACHUSETTS INSTITUTE
OF TECHNOLOGY

MAR 2 6 1996

ARCHIVES

LIBRARIES

Sputter Deposition of Aluminum Nitride
for Applications in Thin-Film Resonators

by
Rajan Sharad Naik

Submitted to the Department of Materials Science and Engineering
on January 19, 1996 in partial fulfillment of the
requirements for the degree of
Master of Science
in Materials Science and Engineering

Abstract

There is considerable interest in developing on-chip, CMOS compatible bandpass filters for applications in the RF communications industry. Filters can be realized from a network of thin-film resonators. Piezoelectric aluminum nitride is the material of choice for the resonator.

A Perkin-Elmer dc magnetron sputtering system is used for low-temperature growth of columnar, c-axis oriented films. A resonator with a center frequency of 1.8GHz requires approximately 1μm of aluminum nitride. The initial film quality, as measured by the X-Ray Diffraction intensity and Full-Width at Half-Maximum of the rocking curve indicated that the films were amorphous. Little improvements were seen after the deposition conditions were varied. Further analysis with Rutherford Back Scattering and X-Ray Photo-Spectroscopy revealed the presence of as much as 15 atomic percent of oxygen.

Consequently, the system was modified to minimize all possible sources of oxygen contamination. The film quality improved with decreasing levels of oxygen contamination. The system can now be used to repeatedly grow (002) textured films on silicon substrates with a rocking curve of 3.5 degrees and 1.5 atomic percent of oxygen. The results of this project show that every effort must be made to minimize the incorporation of oxygen contamination if columnar, highly oriented aluminum nitride films are to be grown.

Thesis Supervisor : L. Rafael Reif

Title : Director, Microsystems Technology Laboratories
Professor, Department of Electrical Engineering and Computer Science

Acknowledgments

This work could not have been possible without the help of a multitude of friends and family. I would like to thank all members of the MTL laboratory, especially Octavio Hurtado for his advice in installing the argon gas lines and frequent bursts of laughter which always kept us going. Joe Walsh always provided first-rate technical support and assisted me greatly in making all the hardware modifications. Thanks also go to Pat Burkhart, Brian Foley, Joe Dimario, Bernard Alamariu and Linus Cordes for their constant willingness to lend a helping hand.

All members of the Reif research group deserve a special mention : 'Master' Weize Chen, perhaps the most intelligent person I know, must be thanked for his insight and ideas and for his companionship during our month of struggle studying for the qualifier exams; Ben 'neck' Tao for being a great office-mate and computer consultant; Simon Karecki for providing all the parties which kept us going through the long, winter months; Alex Cherkassky for preparing us by asking the toughest questions during presentations; Ken 'twins' Liao for introducing me to the group and helping me settle in; Julie 'giggles' Tsai for uplifting all our spirits with her sense of humor and Andy 'hit-man' Tang for being a great friend and partner during all those very long nights in the lab.

None of this research could have been accomplished without all the great virtues of my advisor, Professor Rafael Reif. Thank you for believing in me as a researcher, for all the advice, both technical and otherwise and for the constant support and notes of encouragement. I hope to see you in Zimbabwe for your second honeymoon !

Murthy Nukala and Samir Menon must be thanked as my roommates for all the constant arguments and discussions which no doubt stimulated our intelligence and made me look forward to going home every night. I wish them the best of luck in their great futures. An immeasurable amount of thanks must go to Sridevi Sarma for providing companionship, and nutritious dinners whenever I was too tired to cook for myself ! The world could do with many more such talented, gracious people.

I dedicate this thesis to the three members of my family : my father, Sharad, for being a role model, for showing me how to fight for one's life, for being a fine example of a gentleman, husband and father; my lovely mother, Kusum, for raising me well, for being a friend, and for being the 'rock' of our family while I study abroad; and my brother, Sundip, for being my best friend and for all his remarkable qualities which make it an honor for me to be his brother.

Contents

Abstract 2

Acknowledgments 3

List of Figures 5

List of Tables 6

1 Introduction 7
- 1.1 Applications of thin-film resonators in filters 8
- 1.2 Motivation for using aluminum nitride 11

2 Thin-film resonators 12

3 Reactive sputtering 15

4 Film characterization 18
- 4.1 X-Ray Diffraction 19
- 4.2 Rutherford Back Scattering 20
- 4.3 X-Ray Photo Spectroscopy 20
- 4.4 Scanning Electron Microscopy 20

5 Perkin-Elmer dc magnetron sputtering system 21
- 5.1 System components 22
- 5.2 Gas delivery systems 23
- 5.3 Initial deposition conditions and film quality 23

6 Modifications to system 30
- 6.1 Installation of RGA and hardware modifications 31
- 6.2 Subsequent deposition conditions and film quality 34

7 Conclusions and future work 37

Appendix 39

Bibliography 43

List of Figures

Figure 1	Portable communication transceiver.	8
Figure 2	Pole ladder filter and filter loss characteristics.	9
Figure 3	Thin-film resonator structure.	10
Figure 4	Simplified thin-film resonator model.	14
Figure 5	dc sputtering system and plasma potential.	16
Figure 6	Zone models.	17
Figure 7	Rocking curve schematic.	19
Figure 8	Perkin-elmer dc sputtering system.	22
Figure 9a	Run 12 SEM micrograph.	25
Figure 9b	Run 12 X-ray diffraction measurements.	25
Figure 10	X-ray diffraction measurements versus pressure.	27
Figure 11	Rutherford back-scattering spectrum of initial runs.	27
Figure 12	Effect of oxygen contamination due to an increase in pressure.	29
Figure 13	SEM micrograph showing formation of Al_2O_3.	29
Figure 14	Schematic of water supply to chamber table.	32
Figure 15	Run 74 X-ray diffraction measurements.	34

List of Tables

Table 1	Initial sputtering parameters.	24
Table 2	Typical present deposition parameters.	34

Chapter 1

Introduction

1.1 Applications of thin-film resonators in filters :

There is a great industrial interest in the fabrication of an integrated RF bandpass filter with a center frequency of 1.8GHz for low power portable communication systems (PCS). The anticipated growth of the PCS industry, fueled by emerging economic areas such as Asia and South America, has created a demand for wireless products which have longer operating times and smaller dimensions. Although there is much research in extending the battery lifetime, creating a low power filter is a viable method to achieve the same result.

Figure 1 shows a simplified diagram of the RF section of a wireless communications system. A filter is needed in the receive path to select the signals at the specified frequency, and a filter is needed in the transmit path to select the frequency of the outgoing signal. Current PCS's utilize an off-chip high permittivity ceramic transmission line filter. The size of the filter depends on the electromagnetic propagation velocity within the material. For the specified frequency of 1.8Ghz, the size is typically $1in^3$. An on-chip, integrated circuit CMOS process compatible filter would be smaller and consume less power.

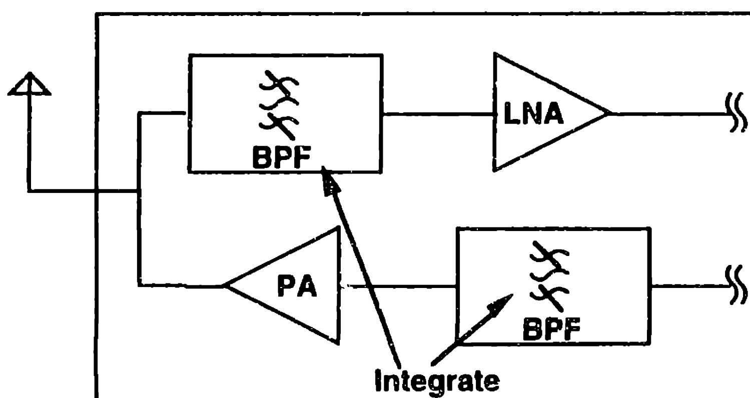

LNA = Low-Noise Amplifier, BPF = Band-Pass Filter, PA = Power Amplifier

Figure 1 : Portable communication transceiver.

A bandpass filter can be realized from a collection of thin-film resonators. Shown in Figure 2 is a seven pole ladder filter with its insertion loss characteristics. Comprehensive models exist to extrapolate such data [1] . It is obvious that the essence of the filter is the thin-film resonator (TFR). The resonating action of a TFR is due to the propagation of an

acoustic wave through a piezoelectric material. Piezoelectric resonators have been extensively studied since the 18th century [2] and are widely used in quartz watches, ultrasonic detectors, buzzers and so on.

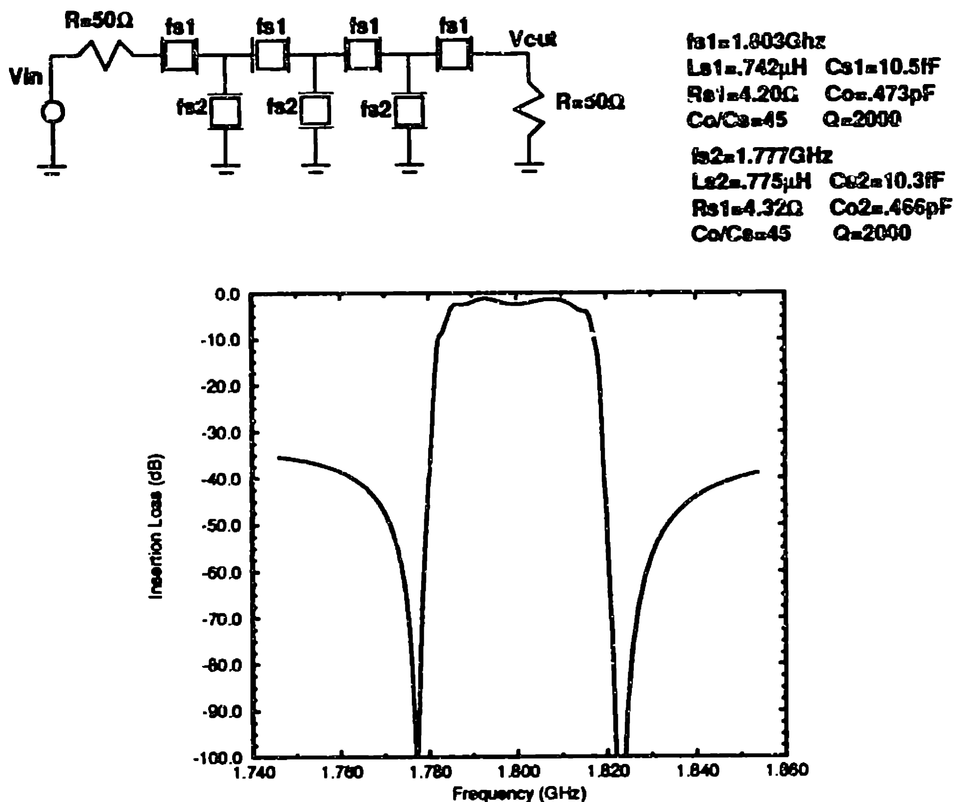

Figure 2 : Pole ladder filter and insertions loss characteristic.

An integrated TFR resonator has been designed here at the Microsystems Technology Laboratories at M.I.T [3] which will specifically use the aluminum nitride films grown in the Perkin-Elmer system. A cross-sectional and plan view of the TFR resonator design are shown on the following page. Needless to say, there are several process details hidden in the figure, such as the use of wafer bonding to create the cavity, the use of Si_3N_4 to act as the supporting membrane, patternability and etchability of the aluminum nitride and so on.

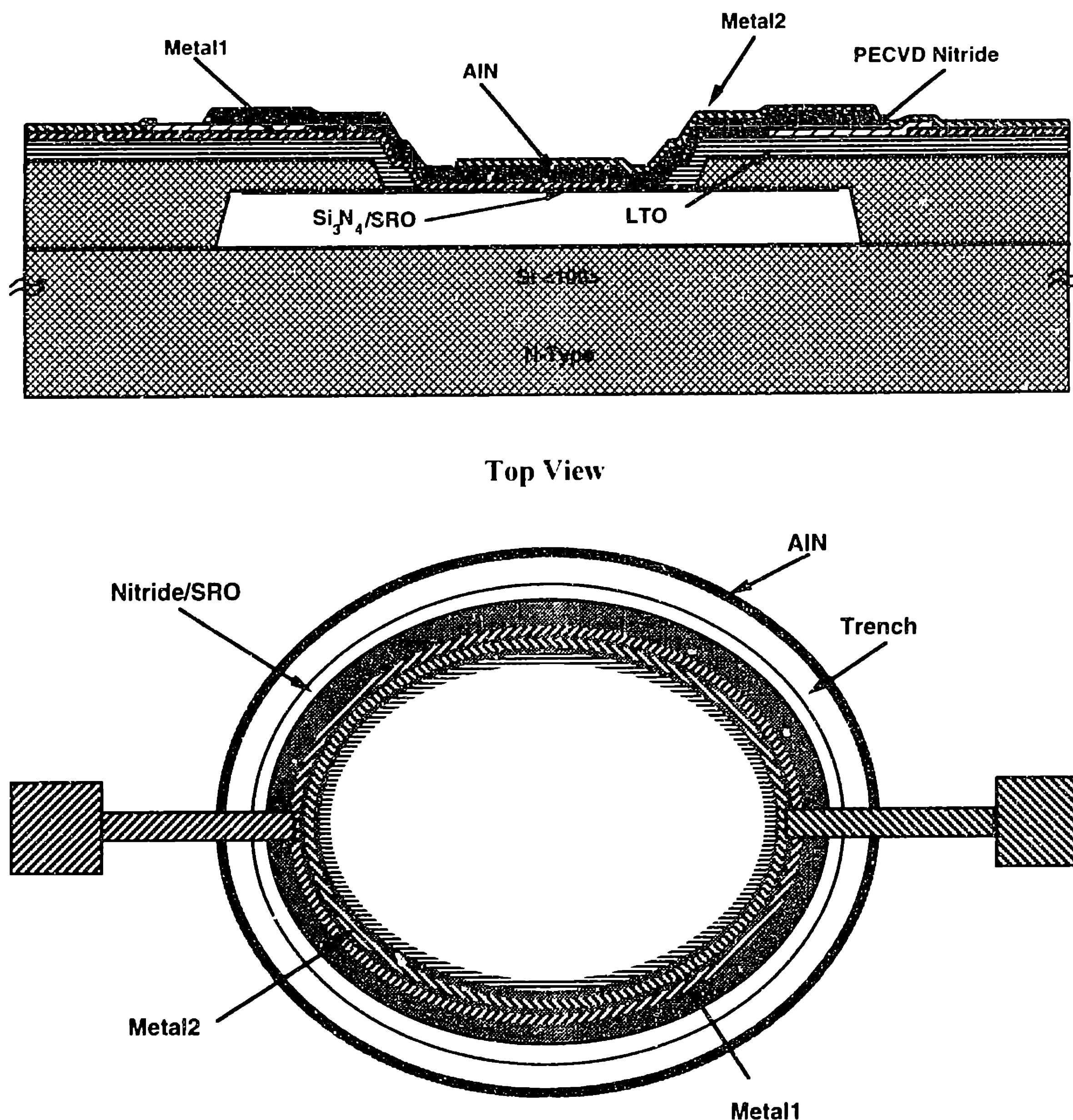

Figure 3 : TFR resonator structure.

In addition to processing issues a large fraction of the TFR design project is devoted to investigating means of tuning the filter. The acoustic velocity through the aluminum nitride film is determined solely by the material stiffness tensor. The wavelength and thus the frequency depends on the film thickness. If many TFR's are to be fabricated on one wafer, maintaining thickness uniformity is crucial. Although thickness, and thus resonant frequency control is possible to within a few percent in a sputtering system, this deviation may be unacceptable for commercial filters. By taking advantage of the non-linear piezoelectric effects, such as the dependence of the piezoelectric stress tensor on

electrostatic stress and mechanical stress, it may be possible to shift the resonant frequency. With some process modifications, the membrane can be stressed by applying a dc bias across it.

1.2 Motivation for using aluminum nitride :

Aluminum nitride is used as the piezoelectric material in this project. The piezoelectric material is the heart of the TFR and consequently of the bandpass filter. Although there are several other highly piezoelectric materials such as quartz and zinc oxide, aluminum nitride is chosen due to the compatibility of its constituent elements in an integrated circuit process. Since aluminum metallization is used as contacts in the fabrication of the TFR, the deposition temperature of aluminum nitride is restricted to below 400°C. Although Molecular Beam Epitaxy (MBE) and Chemical Vapor Deposition (CVD) [4-6] can be used to deposit high quality epitaxial aluminum nitride films, the temperature restriction confines the deposition technique to reactive sputtering. Considering that the melting point of aluminum nitride is approximately 2800°C, thin films deposited by reactive sputtering at temperatures less than 300°C are expected to be small-grained polycrystalline. Naturally, single crystalline films with no defects yield a greater piezoelectric response. However, numerous researchers have successfully deposited polycrystalline aluminum nitride with an almost equivalent piezoelectric response [7]. Furthermore, resonators have been fabricated using polycrystalline aluminum nitride with the required frequency, bandwidth and insertion loss to meet the demands for commercial RF bandpass filters [8-10]. Although resonators have been fabricated, the quality factor, Q, is limited by the presence of grain boundaries, as well as other factors such as the film morphology and losses in the aluminum contacts.

Chapter 2

Thin-Film Resonators

A schematic of a simple TFR is shown in figure 4, together with an electrically equivalent model. An alternating input voltage, or electric field generates an alternating stress within the material via the piezoelectric effect. The alternating stress couples to an oscillatory atomic motion, or in other words, an acoustic wave propagation. At the other aluminum electrode. the oscillatory stress generates an alternating output voltage via the converse piezoelectric effect. Resonance occurs when the transducer thickness is an odd multiple of half wavelengths. Although higher modes propagate, the fundamental mode is the dominant. Thus, only certain frequency signals are allowed to pass. In the equivalent circuit, C_O represents the parallel plate electrical capacitance of the structure, L_S and C_S are associated with the acoustic wave and R_S represents the acoustic and electrical losses.

For more complicated resonator designs such as the monolithic crystal filter correspondingly more complicated equivalent circuits are needed to model the behavior [11] . Although electrical models can predict the resonant frequency and insertion losses, they provide little insight to the resonator behavior. The propagation of acoustic waves through a piezoelectric medium can be modeled from physical principles using a damped harmonic oscillator model. Although feasible, the model is severely complicated due to the fact that the medium is three dimensional and has tensors instead of simple scalars for the stiffness, piezoelectric strain and dielectric constants. A one-dimensional analysis [12] of the TFR is presented in the Appendix, as well as the relationships between the equivalent circuit parameters and materials parameters. Two of the key performance parameters of the TFR are the quality factor Q and the absorption α.

Ideally, an epitaxial film is desired such that no acoustic scattering occurs from defects such as grain boundaries. As stated previously, low temperature growth is required. Sputtering produces polycrystalline films. Films with a preferred orientation, or texture, are preferred since the material tensors are a function of the crystallographic orientation. For aluminum nitride the [002] orientation, or c-axis normal to the substrate, has one of the highest piezoelectric coupling coefficients and can also be preferentially deposited over other orientations.

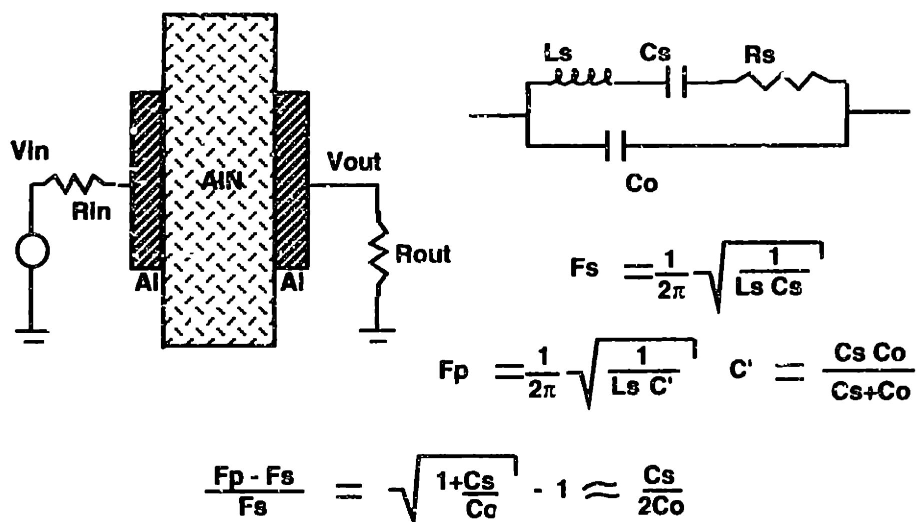

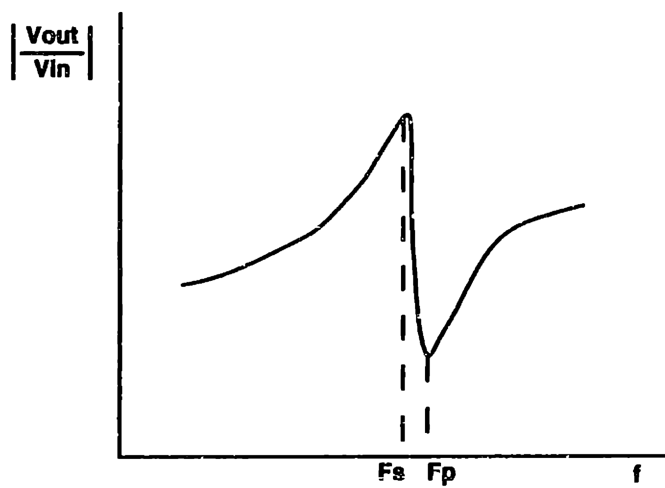

Figure 4 : Simplified TFR electrical model.

Chapter 3

Reactive Sputtering

Low temperature growth of aluminum nitride is achieved by RF or DC reactive sputtering. In the dc case, a negative bias is applied to an aluminum target with respect to the wafer holder. A mixture of argon and nitrogen is introduced and a plasma is formed. Positively ionized argon and nitrogen particles bombard the target, ejecting a mixture of ionized and neutral aluminum particles. These particles, after suffering many collisions, adsorb on the wafer surface, react with nitrogen particles and heterogeneously nucleate into two-dimensional aluminum nitride grains. A dc sputtering system together with the plasma potential diagram is shown below.

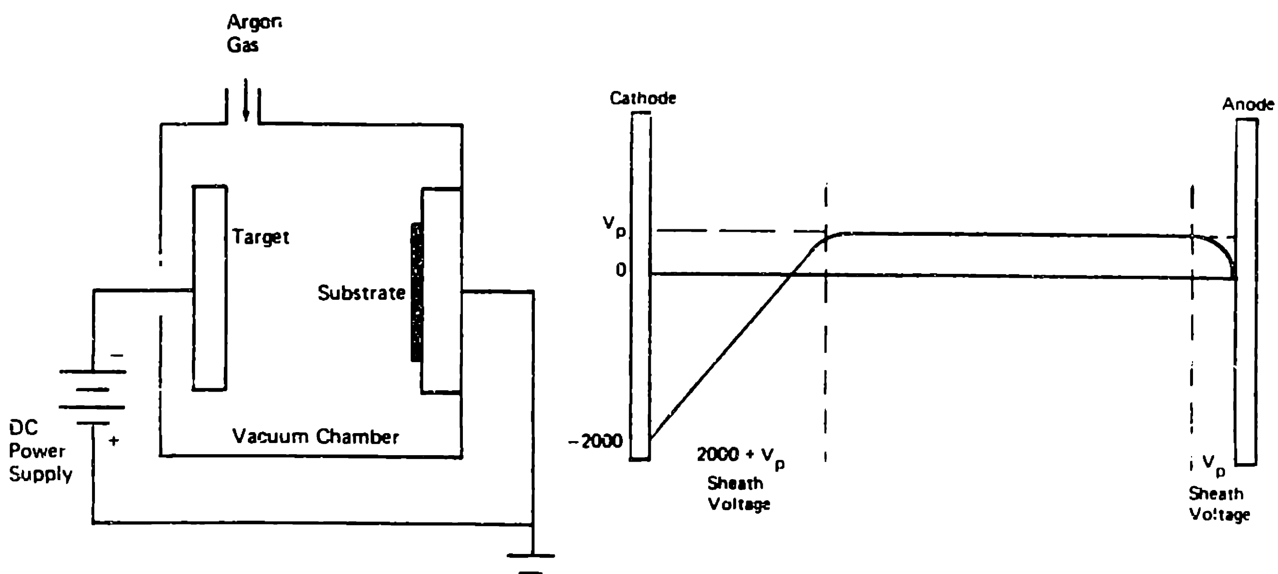

Figure 5 : dc sputtering system and plasma potential.

RF sputtering is used whenever insulating films are grown. Consider depositing highly insulating aluminum nitride using a DC system. Initially, the target is at a negative bias, -V_S. As the process continues, it is conceivable that the target becomes 'nitrided', or in other words, aluminum nitride forms on the target. The target subsequently accumulates positive charge due to loss of electrons as the incoming positive ions are neutralized at the surface. The target bias subsequently rises to 0 volts and the discharge is extinguished. By using an ac discharge, the positive charge accumulated during one half-cycle is neutralized by electron bombardment during the next half-cycle. In order to keep up with the rate of charging, an RF frequency greater than approximately 1MHz is needed.

Typically, 13.56MHz is the frequency allotted by the FCC to avoid interference with communications [13].

Once the grains nucleate, the developing grain structure is a strong function of the deposition temperature and pressure. The classic theory of grain growth [14, 15] by sputtering is summarized here. Under conditions of low homologous temperature and high pressure adatoms have low surface mobility due to reduced energy and reduced mean free path. Subsequently, the adatoms cannot diffuse to preferred lattice sites. This region is known as Zone 1, characterized by small, columnar grains with domed tops. Zone 2 is associated with larger grains and a smoother surface due to the increased mobility. Zone 3 is associated with extremely large grains, possibly single-crystal films. In this zone, considerable grain growth by grain boundary motion occurs during deposition due to the high temperatures and low pressures. Just as in sputtered metals aluminum nitride grows in a preferred orientation, usually the [002] orientation (c-axis of the hexagonal cell perpendicular to the substrate) since it has the lowest surface energy. However, other orientations can be selectively grown as well [16].

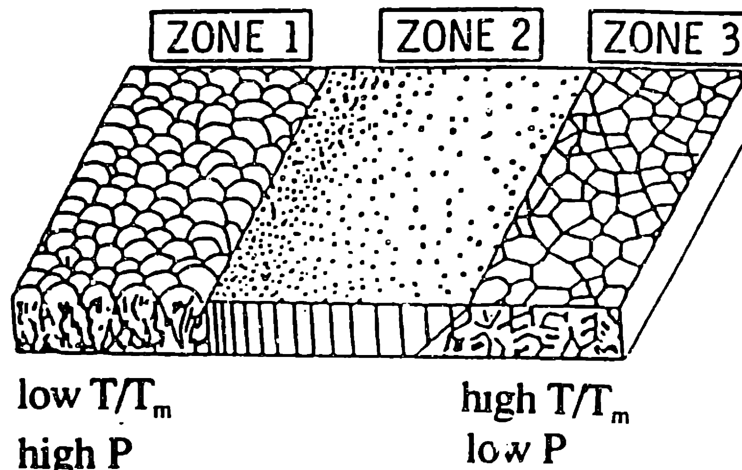

Figure 6 : Zone models.

Chapter 4

Film Characterization

4.1 X-Ray Diffraction :

X-Ray Diffraction is the first tool used to characterize the film quality. A collimated x-ray beam incident on the sample is reflected from successive atomic planes. If the path difference between the reflected beams is a whole multiple of the wavelength,

$$n\lambda = 2d\sin\theta$$

constructive interference occurs with a peak in intensity. A θ-2θ scan refers to the situation where the sample and detector are rotated such that the angle between the source and sample is always θ and the angle between the sample and detector is always 2θ. This scan identifies which of the polycrystalline phases are present. The intensity of the peaks is an indication of the degree of crystallinity. An amorphous film will have several low-intensity peaks whereas a textured film will have a single high intensity peak. In addition to a θ-2θ scan, the FWHM of the rocking curve is measured.

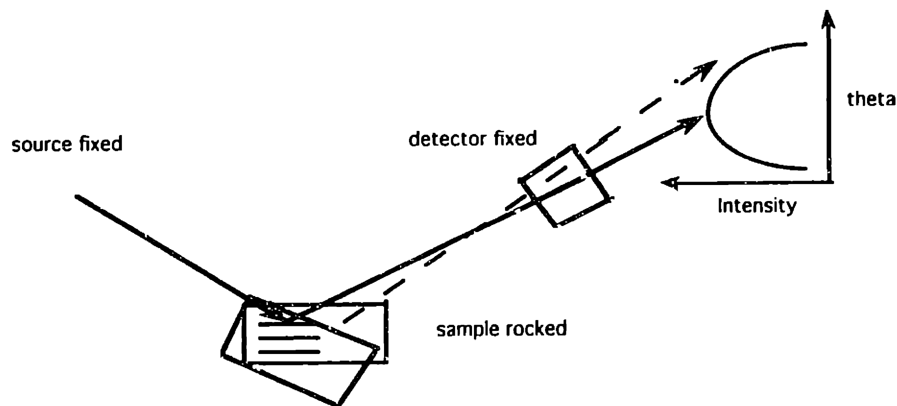

Figure 7 : Rocking curve schematic.

The detector is fixed at the 2θ angle of the desired peak and the sample is 'rocked' about the θ axis. As the θ axis approaches the point where Bragg scattering occurs, the intensity rises. As the θ axis rotates past the Bragg angle, the intensity falls. The subsequent intensity profile gaussian in shape and the width at half the intensity is the FWHM. A perfect single crystal will have a FWHM equal to the resolution of the detector, which is typically a few tenths of a degree. A textured crystal will have a FWHM that correlates with the range of orientation since the Bragg condition will be satisfied over a wider range of angles centered around 2θ [17] .

4.2 Rutherford Back Scattering :

Rutherford Backscattering Spectroscopy (RBS) employs high energy (1-4MeV) helium ions to determine the concentration profiles as a function of depth. Upon collision with the sample atoms, the helium ions back-scatter elastically. The energy loss of the helium ions is a function of the sample atom characteristic and distance from the surface. Both elemental analysis and distribution are determined from the back-scattered helium ions. The sensitivity of RBS to light elements is poor. The minimum detection limit of this technique is approximately $5E18cm^{-3}$ or 0.01 atomic %.

4.3 X-Ray Photo Spectroscopy :

X-Ray Photo-Electron Spectroscopy (XPS) is a tool used to measure the stoichiometry and impurity ratios. Surface charging on the aluminum nitride by electrons is avoided by using XPS instead of Auger Electron Spectroscopy (AES).The sample is introduced into a high-vacuum chamber, and 1-2keV x-rays from a magnesium source impinge the sample surface. Photoelectrons are ejected from the surface. The measured energy of the ejected electron at the spectrometer E_{sp} is related to the binding energy E_b, referenced to the Fermi energy E_f by :

$$E_b = h\upsilon - E_{sp} - q\phi_{sp}$$

where hv is the energy of the primary X-rays and ϕ_{sp} the work function of the spectrometer (3 to 4eV). The spectrometer and sample are connected forcing the Fermi levels to match. Elemental as well as chemical analysis is possible. XPS sensitivity is approximately 0.5 atomic %. In combination with a in-situ argon sputtering gun, depth profiling of the film is possible.

4.4 Scanning Electron Microscopy :

A Zeiss DSM 982 Gemini Scanning Electron Microscope (SEM) with an in-lens detector is used to examine the surface and cross-section appearances of the film. If the films are coated with a thin layer of platinum, approximately 200Å resolution is achievable. A relatively low electron potential of 5kV is used to further minimize charging effects.

Chapter 5

Perkin-Elmer dc magnetron sputtering system

The following paragraphs describe the state of the system and deposition conditions as they were when the project was started. The system is physically located in the class 100 clean room at the Microsystems Technology Laboratories at the Massachusetts Institute of Technology.

5.1 System components :

A schematic of the Perkin-Elmer model 4410 sputtering system is shown below. There are three basic components namely the load lock, chamber and target assembly.

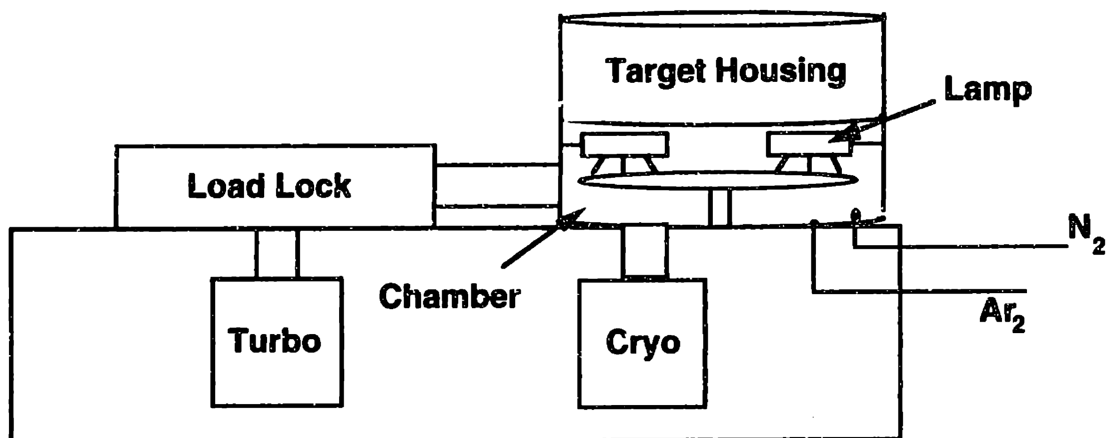

Figure 8 : Perkin Elmer dc sputtering system.

The load lock is separated from the chamber by an O-ring sealed isolation door. A 36.7 CFM mechanical roughing pump and a Leybold turbomolecular pump maintain the load lock base pressure in the high 10^{-8} torr range as monitored by an ion gauge and convectron gauge. The load lock is fitted with a 23 inch diameter wafer pallet capable of holding thirteen 4-inch wafers. The wafers are loaded horizontally face-up on the pallet which is then lowered onto a set of carrier rails. A transport motor serves to move the pallet into the chamber once the required base pressure is achieved.

The chamber is pumped on by a Cryogenics cryogenic pump through a 10-inch diameter baffle valve. An aluminum annular water-cooled table with a stainless steel ground shield rests in the center of the chamber above the baffle valve. The copper water lines are fed in through a differentially pumped, rotary O-ring seal feedthrough which allows the table to be rotated as well as moved vertically so that the target-substrate spacing can be varied.

When the isolation door is opened, the pallet is moved into the chamber and temporarily sits on another set of rails in the chamber. The table is then raised and lifts the pallet above the carrier which is then moved out of the chamber. A collar runs around the stainless steel chamber walls and supports a set of three infrared lamps which are used to bake the chamber or to heat the wafers directly below. Up to 1500W of power is supplied to the lamps via a metal-ceramic feedthrough in the base of the chamber. During deposition, the pressure is maintained by the baffle valve. When fully open, the cryogenic pumping speed is at a maximum and the pressure is at a minimum for a given flow rate. When fully closed, the pumping speed is at a minimum and the pressure at a maximum for a given flow rate. The deposition pressure is monitored by a MKS baratron gauge whose output is fed back to the electronically controlled baffle valve for accurate pressure control. A base pressure in the low 10^{-8} torr range is achievable in the chamber.

Situated above the lamps is the target assembly. Five kilowatts of dc magnetron power are supplied to 99.999 % pure copper, chromium and aluminum delta targets. The magnet assembly together with the cooling water supply are located above each target. Below the targets is a delta-shaped target shutter which can be rotated to expose any one target to the wafers. The O-ring sealed target assembly can be hoisted up in order to gain access to the chamber interior.

5.2 Gas Delivery Systems :

Six-nines purity tank nitrogen and four-nines purity house argon are the gases delivered to the system. The load lock can be vented with a house nitrogen feedthrough in the base of the load lock. Tank nitrogen and house argon are fed into the chamber via stainless steel lines through Nupro valves and mass-flow regulators. The length of line from the chamber to the tank nitrogen is approximately 40 feet, and the length of line from the chamber to the house argon is well over several hundred feet.

5.3 Initial deposition conditions and film quality :

The initial depositions of 1μm aluminum nitride were performed under the conditions outlined in table 2. (100) silicon, sputtered aluminum, silicon oxide and silicon nitride were used as substrates. In the case of the silicon substrates, the native oxide was removed with a fifteen second dip in dilute (5%) Hydrofluoric acid. If the heat lamps were to be used, the temperature in the chamber was allowed to equilibrate at least thirty

minutes before introducing the wafers. When the pressure in the load lock was in the 10^{-8} torr range, the platten was moved into the chamber. The pre-deposition procedure was executed, followed by the actual deposition. The 30 minute argon plasma served to remove any native aluminum oxide on the target surface, and the 30 minute target condition served to equilibrate the target surface before rotating the target shutter and exposing the wafers to the plasma.

Although aluminum nitride is an insulator, dc sputtering is possible. Indeed, aluminum nitride does form at the target surface however the plasma was not observed to extinguish during a deposition. This may be due to the fact that the aluminum nitride does not fully cover the target and so is never perfectly insulating. However, if many depositions were done in a pure nitrogen plasma, it became progressively difficult to sustain the plasma since a thicker layer of aluminum nitride forms on the surface. To prevent this, target surface cleans were done in a pure argon plasma immediately before all depositions to sputter away any surface aluminum nitride.

Power (kW)	1
Pressure (mtorr)	2
Temperature (°C)	100-250
Gas flow rate (sccm)	25
Gas composition (N_2 %)	50-100
Substrate rotation	yes
Deposition rates (µm/hr.)	0.3-0.6
Pre-deposition procedure	30 min. Ar plasma shutter closed, 30 min. target condition.

Table 1 : Initial sputtering parameters.

The X-ray results of these initial runs suggested that the film quality was poor. Often, multiple peaks existed or a very low intensity [002] peak existed. There was no noticeable improvement with changes in temperature, gas composition and flow rate. However, the film quality seemed to be best on silicon substrates and worst on aluminum substrates. A sample X-ray scan, rocking curve and cross-sectional SEM are shown on the following page for a silicon substrate.

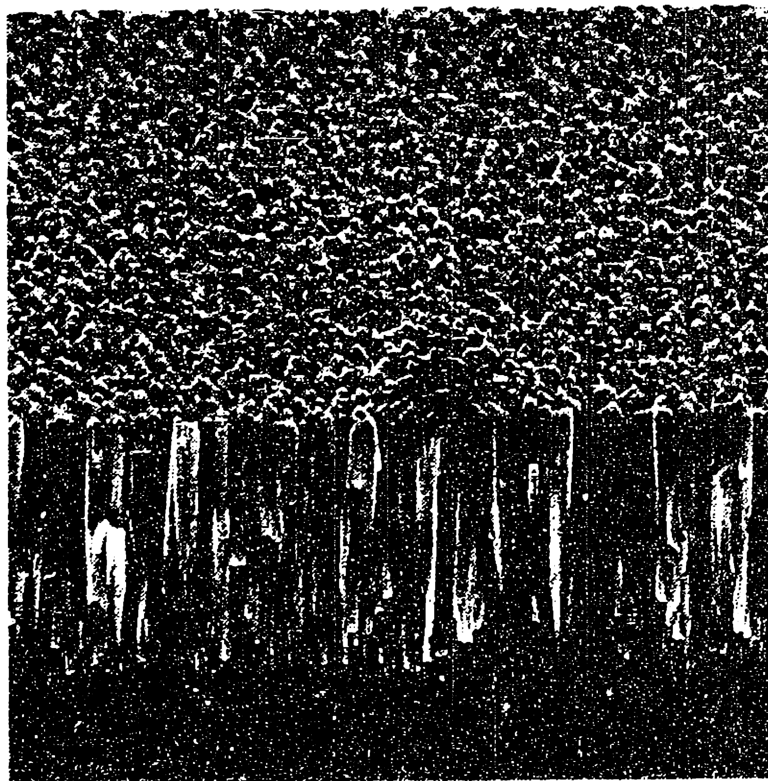

--- = 500Å

Figure 9a : Run 12 SEM.

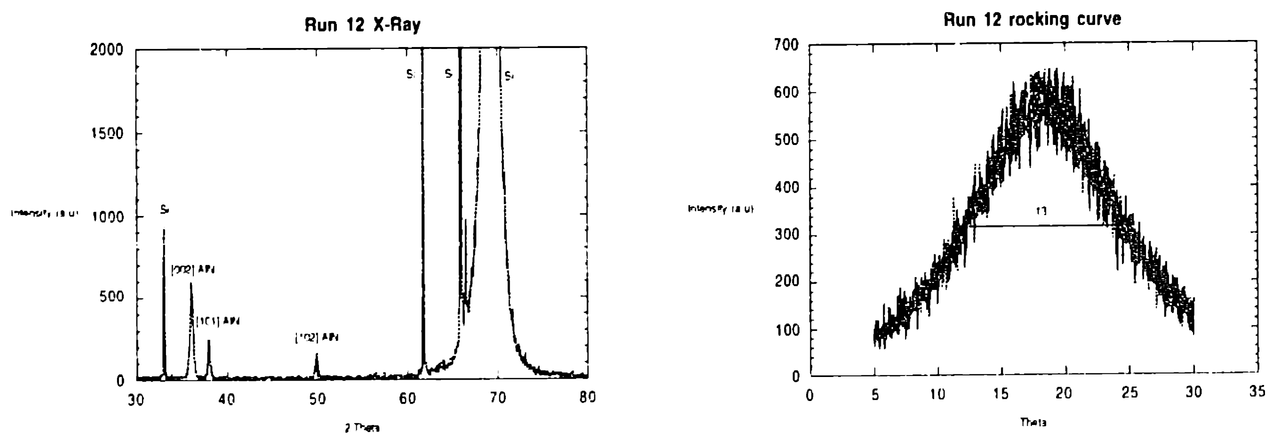

Figure 9b : Run 12 XRD.

It is generally thought that for the film to show any piezoelectric response, a single high-intensity [002] peak with a FWHM of less than 4° is required. For comparison, Motorola's high temperature (800°C) sputtered aluminum nitride on silicon oxide was characterized at the same X-Ray power. The single [002] peak had an intensity of approximately 100 000 counts and the FWHM was 2°.

It was decided next to investigate whether decreasing the target-substrate spacing *d* made any improvements. The motivation for this change was that the deposition rate would increase and that adatoms would have more mobility as the effective mean free path would be increased. It was necessary to remove the lamps in order to be able to move the table up higher. Since the melting point of aluminum nitride is greater than 2000°C it is unlikely that a few hundred degrees will assist in grain boundary motion or film quality enhancement. Moreover, no effect of temperature on the film quality was seen in the previous experiments.

The X-ray results of these next set of experiments were equally bad. It was then decided to increase the deposition rate by not rotating the wafers. Each wafer was exposed to the plasma under the aluminum target directly for 30 minutes. The table was then rotated to move the wafer out of the plasma and bring in another wafer under the target. The deposition rate per wafer increased to approximately 1.5µm/hr. No noticeable improvement was seen. A series of runs were then done at various pressures. Surprisingly, the deposition rate did not decrease as the pressure was varied from 2 mtorr to 10 mtorr. However, the film quality degraded tremendously as measured by the XRD intensity of the [002] peak.

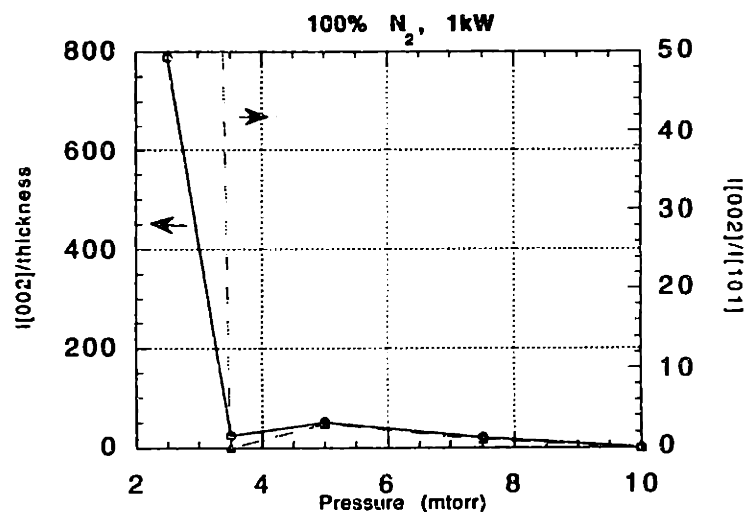

Figure 10 : XRD intensities vs. pressure.

Next, the deposition rate was varied with the dc power. The deposition time was adjusted such that approximately 1μm aluminum nitride was grown for all runs. Again, no improvement was seen either at low power or high power. At this point, it was realized that the solution to obtaining good films was more fundamental in nature and not process related. Consequently, RBS was used to examine the films. A typical spectrum together with the simulation is shown below.

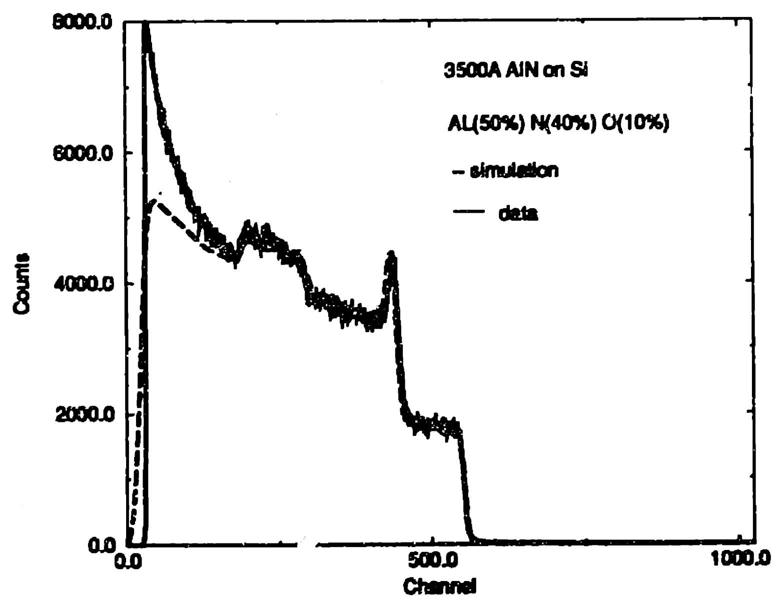

Figure 11 : RBS spectrum of initial runs.

It was not possible to simulate a good fit by varying the thickness or the stoichiometry. However, after accounting for the presence of small concentrations of oxygen, the simulation fitted the data much better. An exact measure of the amount of oxygen was not possible because oxygen and nitrogen have similar masses and their individual contributions to the spectrum overlap considerably, making resolution difficult.

XPS was used next to extract an oxygen concentration of about 15 atomic %. The aluminum/nitrogen ratio was approximately 1.1. With a base pressure of 3×10^{-8} torr, it was hard to believe that such high levels of contamination existed in the films. The oxygen content in the films was measured as a function of the deposition pressure, and the results shown below. It is now apparent why the deposition pressure had no effect on the deposition rate and why the film quality decreased with pressure. Assuming

$$\lambda = \frac{kT}{\sqrt{2}\pi a^2 p} \qquad\qquad f = 1 - \exp\left(-d/\lambda\right)$$

where λ is the mean free path and f is the fraction of atoms that experience at least one collision before reaching the substrates, at 2 mtorr these values are 1.7cm and 99.6% respectively. At 10 mtorr, they are 0.3cm and 100% respectively. In other words, increasing the pressure does not significantly decrease the energy of the adatoms on the surface. However, the deposition pressure is maintained by baffle valves inbetween the cryogenic pump and the chamber. For a high deposition pressure, the valves are more closed, thereby the pumping speed of the cryogenic pump is reduced. If the pumping speed of the cryogenic pump is reduced, the base pressure in the chamber is increased as well as the residence time of all the particles. So, in conclusion, the detrimental effect of high deposition pressures was due to a decrease in the pumping speed, a subsequent increase in the base pressure and a higher oxygen concentration in the films. The reduction in surface mobility was not the cause as the zone model predicts. XPS measurements of the oxygen concentration in films grown at high pressure supported this claim, as shown on the following page.

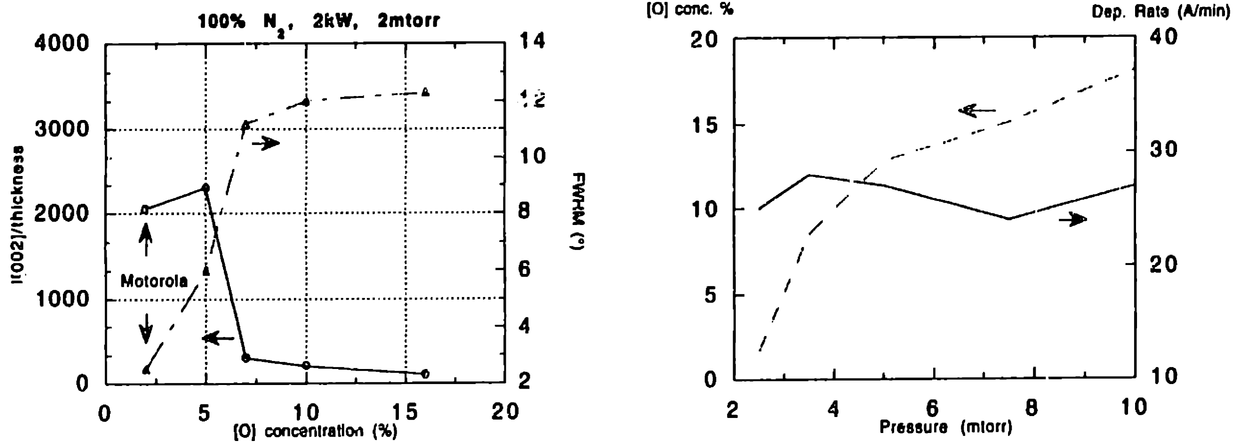

Figure 12 : Effect of oxygen contamination due to increase in pressure.

It was interesting to see in the SEM cross sections the formation of the [111] planes of Al_2O_3 in films with high oxygen concentrations.

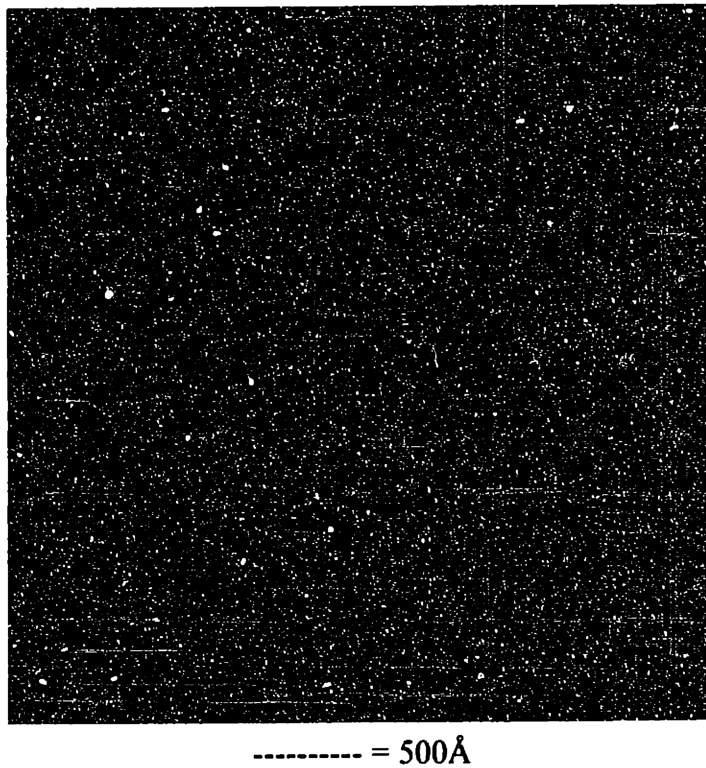

---------- = 500Å

Figure 13 : SEM showing formation of Al_2O_3.

Chapter 6

Modifications to the system

6.1 Installation of RGA and hardware modifications :

By experimenting with the pre-deposition procedures, it was thought that the oxygen contamination could be reduced. Specifically, the chamber was exposed to an argon plasma while the wafers were in the load lock. The sputtered aluminum would act as a getter and reduce the base oxygen pressure before deposition commenced. Many variations of this procedure were tried. The length of the argon plasma was varied as well as the power. A pre-deposition nitrogen plasma was also tried with many variations. Unfortunately, the oxygen content in the films remained within 5 to 10 atomic %. Assuming that the source of oxygen is degassing from the chamber walls, and that

$$P=[O]RT \qquad J=[O]\frac{c}{4} \qquad \frac{1}{2}mc^2=\frac{3}{2}kT$$

where [O] is the oxygen concentration, *J* the atomic flux onto the substrate and *c* the average thermal velocity in the plasma, the oxygen content in the films is :

$$[O]\propto\frac{P}{(dep.rate)T^{1/2}}$$

From the calculation, an oxygen partial pressure of approximately 1×10^{-8} torr is needed to explain a film oxygen concentration of 10 %. This analysis suggested that although our chamber base pressure was 3×10^{-8} torr, most of the constituents were oxygen. In order to examine this issue, a Leybold Inficon Residual Gas Analyzer (RGA) was attached on one of the chamber ports with a copper O-ring seal. Indeed, the RGA indicated that 95% of the chamber consisted of water vapor. The two possible sources of water were the cooling lines above the targets and the cooling lines that ran within the table. The entire table assembly was removed and inspected. As described previously, a water-in and water-out line entered the chamber from the rotary feedthrough to the table. The water lines entered the table through an o-ring seal seated on a copper flange as shown below. The chamber was leaky due to a scratch in the copper flange which prevented the o-ring from sitting flush against the flange.

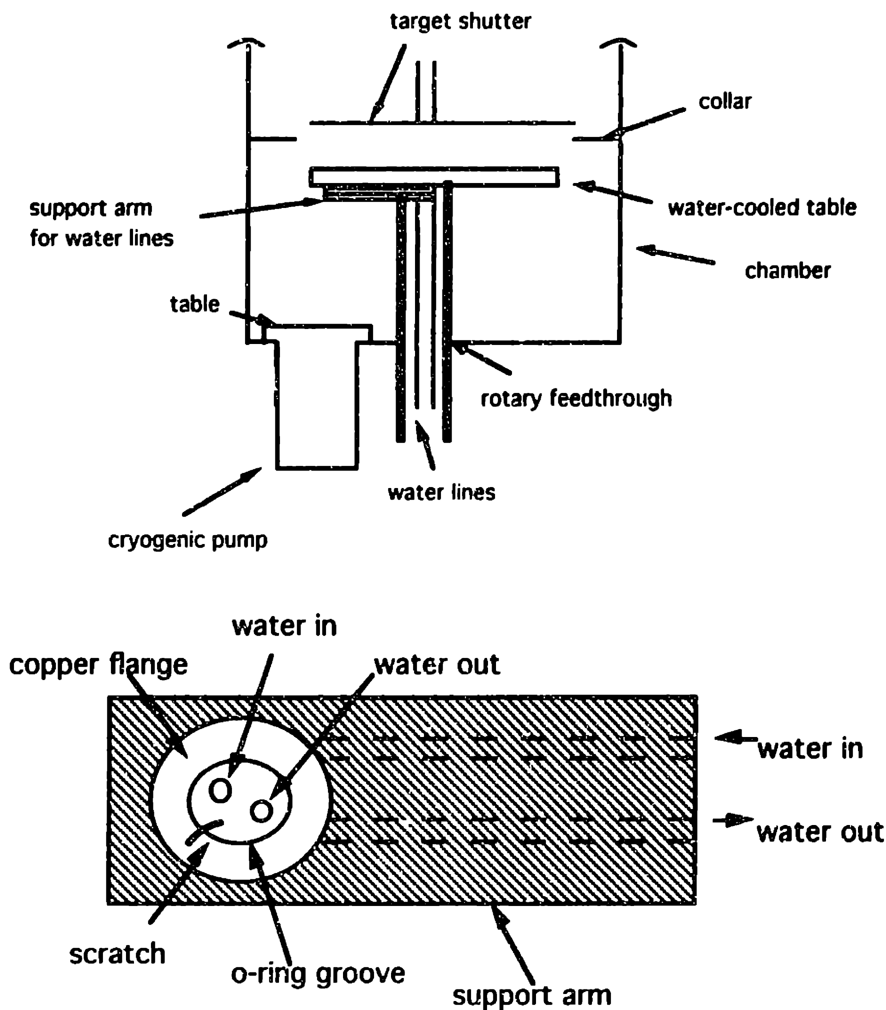

Figure 14 : Schematic of water supply to table.

The copper flange was polished to remove the scratch and the table assembly rebuilt. However, the RGA indicated that the leak was still present. This may have been due to the fact that polishing thinned the flange to the extent that the flange and not the o-ring was contacting the table when the system was re-assembled. Even after a slightly larger o-ring was inserted, the leak was still present. It was decided next to remove the water supply and instead run house nitrogen gas through the water lines. The cooling action of the water was not necessary as the temperature during deposition due to plasma heating was approximately 100°C. The base pressure of water decreased slightly after this modification. It was thought that a substantial amount of water still existed in the copper

lines and was being carried into the chamber by the nitrogen. During this maintenance schedule, the rotary feedthrough developed a leak. This was evident as the base pressure, monitored by the chamber ion gauge, increased periodically as the table rotated. There was a great incentive to remove the rotary feedthrough assembly as well as the water-cooled table. A simple stainless steel flange was used to close the chamber once the assembly was removed. Depositions would now be accomplished by moving the platten into the chamber and leaving the carrier in the chamber so that the platten rested on the carrier instead of the table. It was still possible to close the isolation door with the carrier in the chamber. It was also decided at this point to re-install the lamps in order to assist in bake-out of the chamber during pump down.

After all those modifications, the partial pressure of water in the chamber decreased by an order of magnitude. It was expected that the total base pressure would decrease by approximately the same amount as the water leak constituted a large fraction of the total base pressure. However, during the course of the modifications a minor leak to the atmosphere developed in the target shutter rotation assembly. Consequently, the chamber base pressure remained in the low 10^{-8} torr region, however most of the constituents were now atmospheric nitrogen. This improvement came at the expense of losing rotation capability since the rotation feedthrough was removed. However, subsequent depositions still had 5 atomic % of oxygen and unacceptably low XRD intensities. At this time, the purity of the gas lines were tested with the RGA. The nitrogen line was expectedly clean as the source was a tank of ULSI grade (99.9999 % pure) nitrogen. The argon on the other hand brought with it approximately 1000ppm of water and oxygen combined. If 2 mtorr of argon pressure is used at any time during a deposition, a contaminant partial pressure of 2×10^{-6} torr would exist in the chamber. As shown previously, this level of oxygen species is unacceptable. The high concentration of moisture in the gas lines was due to the fact that the source of argon was the house argon. The entire length of stainless steel lines that fed into the chamber was removed, and new lines were welded in place. A ULSI grade argon tank was purchased and welded onto the new lines. In addition, both the nitrogen and argon lines were baked to remove any adsorbed moisture by wrapping the lines with electrical heat tapes. The length of argon gas line was now approximately 40 feet.

Under typical pre-deposition conditions, the native oxide on the target was removed with an argon plasma. Previously, the table prevented any material from depositing inside the cryogenic pump. In order to prevent the degradation of the cryogenic pump, a 12-inch diameter stainless steel table was constructed with 1 inch feet and seated in the chamber

directly above the baffle valve and cryogenic pump. Although the table would slightly reduce the effective pumping speed, it was preferred to minimize the damage to the pump due to aluminum coatings in the pump interior. The cryogenic pump was also refurbished with new charcoal absorption pads.

6.2 Subsequent deposition conditions and film quality :

Despite the installation of the table above the baffle valve, the chamber base pressure remained in the mid 10^{-8} torr range. A dramatic improvement in the film quality resulted from all the modifications. Typical deposition conditions are shown below :

Pressure (mtorr)	2
Temperature (°C)	100
Gas flow rate (sccm)	20-80
Gas composition (N_2 %)	100
Substrate rotation	not possible
Deposition rates (µm/hr.)	1.5
Pre-deposition procedure	30 min. Ar plasma, chamber exposed. 5 min. target condition.

Table 2 : Typical present deposition parameters.

Under the above mentioned conditions, a high intensity [002] peak and 3.5° FWHM is repeatedly obtainable on silicon substrates. The oxygen content in these films is approximately 2 atomic %.

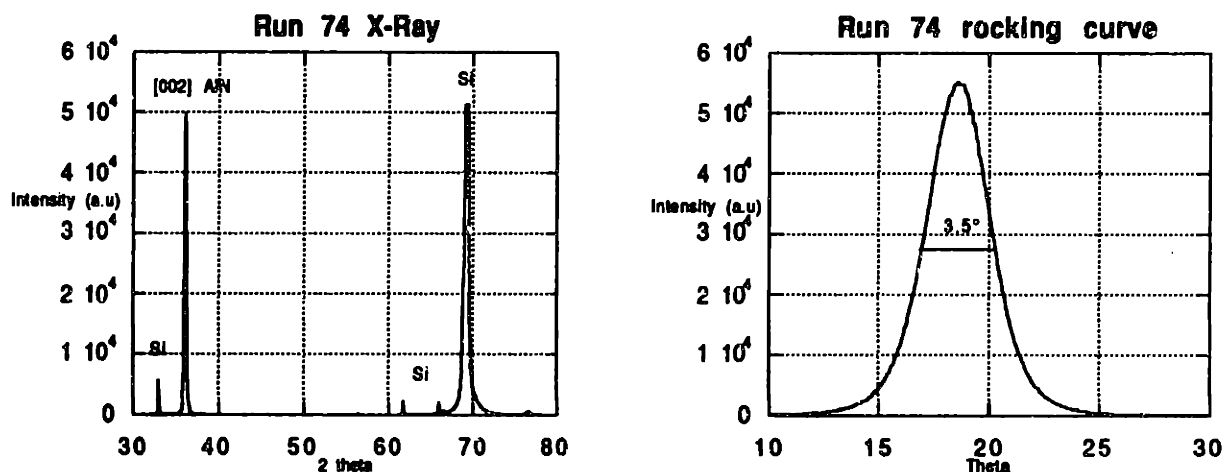

Figure 15 : Run 74 XRD.

The improvement in the film quality is solely due to a decrease in the oxygen content in the films. The pressure is kept as low as possible to maximize the pumping speed and therefore minimize the residence time of any oxygen species. A lower pressure cannot be achieved since the plasma cannot be maintained. The temperature of 100°C is due solely to plasma heating. Using the heat lamps during deposition increases the moisture degassing rate from the walls, so the lamps are never used during deposition. Their sole purpose is to bake out the chamber once it has been exposed to the atmosphere and assist to reduce the pump-down time. The pre-deposition argon plasma which served to remove the native oxide serves another more important function. Prior to the pre-deposition argon plasma, the partial pressure of water and oxygen in the chamber is in the high 10^{-9} torr range. After the argon plasma, the partial pressure drops into the low 10^{-10} torr range through the gettering action of the aluminum deposition on the chamber walls. Previously, this gettering action was damped due to the presence of the table in the chamber which prevented the chamber walls from receiving any aluminum coating. A longer pre-deposition argon plasma does not reduce the oxygen species base pressure further.

For implementation into a TFR design, one of the preferred substrates is aluminum not silicon as the base aluminum can serve as an electrical contact. Using the above deposition conditions, 1μm of aluminum nitride was grown on approximately 1μm aluminum films on silicon wafers. The aluminum was sputtered onto the silicon wafers in a commercial Varian sputtering system. The film quality as measured by the x-ray diffraction intensities was poor despite the fact that the oxygen contamination was less than 2%. It was believed initially that surface roughness of the aluminum prevented any adatom surface migration during deposition leading to amorphous films. Since the absolute surface roughness scales with the film thickness, depositions were then made on aluminum films as thin as 1000Å. The subsequent films were equally poor. Due to aluminum's affinity for oxygen, an amorphous aluminum oxide scale exists on the aluminum films. The amorphous structure possibly prevents any ordered nucleation on its surface leading to amorphous growth of aluminum nitride. To test this hypothesis, silicon wafers were loaded into the load lock, the pre-deposition getter executed, and then approximately 1μm of aluminum was deposited in situ with a pure argon plasma. Nitrogen was then immediately introduced and the argon valve closed so that growth of aluminum nitride could commence. The aluminum nitride film quality on these films was of similar quality to those grown on silicon wafers, although the best rocking curve measured 3.6°. X-ray diffraction measurements on the aluminum films showed them to be highly oriented in the

(111) direction. It is evident that, as with the (100) silicon wafers, there is a quasi-epitaxial relationship with the (002) orientation of the aluminum nitride.

Chapter 8

Conclusion and future work

A Perkin-Elmer dc magnetron sputtering system was modified extensively to be able to deposit high quality aluminum nitride films on silicon and aluminum substrates for potential applications in thin-film resonators. Although the film quality can be improved slightly by varying the deposition conditions, growth of high quality films can only be achieved if the incorporation of oxygen species is minimized. Due to the fact that the deposition rates may be low in order to maintain film uniformity, and due to the fact that aluminum has a great affinity for oxygen, additional precautions must be taken to remove all possible sources of contamination. Growth of highly oriented aluminum nitride films is easier on crystalline or textured substrates.

The film quality can further be improved by varying the power, flow rates and gas composition. It is expected that a rocking curve of less than 2° will be obtainable if further reductions are made in the oxygen content. Heat lamps can be installed in the load lock to bake out the platten before introduction into the chamber since the platten is exposed to the atmosphere during loading and unloading of wafers. Although a few researchers are able to grow high quality films, there does not exist an understanding of why particular deposition conditions lead to good films, and neither does there exist a consensus as to whether the film quality is highly machine dependent, process dependent or both. Consequently, an understanding of the growth mechanisms of highly piezoelectric aluminum nitride is essential. X-ray intensity and rocking curve measurements give information about the crystalline quality of the material, but if the films are to be integrated into a thin-film resonator, some electrical measurements are more appropriate. In addition, other materials factors become important such as the film stresses in such a multi-layered structure, thickness uniformity, grain size, stoichiometry and surface roughness. The realization of a working filter essentially depends on the success of two parts, materials and electrical. A correlation between the materials properties and the electrical performance is necessary.

Chapter 8

Appendix

One Dimensional Acoustic Resonator

It is assumed that the electrodes have no mass, and that the material is isotropic.

e = piezoelectric stress constant
c^E = elastic constant at constant electric field
ε^S = permittivity at constant strain
K = piezoelectric coupling constant
T = stress
u = particle displacement
v = velocity of acoustic wave
V = potential
l = thickness of piezoelectric material

Typically

$$K^2 = \frac{e^2}{c^E \varepsilon^S} << 1$$

Constitutive relations :

$$D = \varepsilon^S E + eS \qquad S{=}\text{strain}$$

$$T{=}c^E S - eE$$

From Newton's Law T=FA, it can be shown that :

$$\frac{\partial T}{\partial z} = \rho \ddot{u} = \rho \dot{v}$$

and that:

$$\frac{\partial v}{\partial z} = \frac{\partial S}{\partial t}$$

In the frequency domain, the above equations become :

$$\frac{\partial T}{\partial z} = j\omega\rho v \qquad \frac{\partial v}{\partial z} = j\omega S \qquad I = j\omega AD$$

Eliminating E, the familiar wave equation is derived :

$$\frac{\partial^2 v}{\partial z^2} + \omega^2 \rho \frac{v}{c^D} = 0$$

where ρ is the material density, and

$$c^D = c^E\left(1 + \frac{e^2}{c^E \varepsilon^S}\right).$$

Assuming the solution consists of two traveling waves : $v = v_F e^{-i\beta z} + v_r e^{i\beta z}$
that the boundary conditions are T(±l/2)=0 and that :

$$V = \int_{-l/2}^{l/2} E dz \qquad \beta = \omega\sqrt{\frac{\rho}{c^D}}$$

where V is the potential along the resonator, the impedance Z = V/I is :

$$Z = \frac{1}{j\omega C}\left(1 - \frac{K^2}{1+K^2}\frac{\tan(\beta l/2)}{(\beta l/2)}\right)$$

where K is the coupling coefficient and C the parallel plate capacitance of the piezoelectric material. The quality factor, Q and absorption α are defined as

$$Q = \frac{f}{2}\left(\frac{d\phi}{df}\right) \qquad \phi = \frac{\beta l}{2} \qquad \alpha = \frac{\omega}{2vQ}$$

evaluated at the resonant frequency.

The connection between the impedance derived above and the simplified TFR model shown in figure 4 follows below.

Resonance occurs at φ=π/2. An expansion of tan φ near π/2 exists :

$$\tan\phi = \sum_{n=0}^{\infty} \frac{2\phi}{\left((n+1)\frac{\pi}{2}\right)^2 - \phi^2}$$

Using the first term of this expansion with the assumption that subsequent resonances are far enough apart such that they do not interfere with each other, it can be shown that :

$$Z = \frac{1}{j\omega C} \frac{\alpha_n^2 - 2K^2}{\alpha_n^2} \left[\frac{1 - \omega^2 \left(\frac{l}{v}\right)^2 \frac{1}{\alpha_n^2 - 2K^2}}{1 - \omega^2 \left(\frac{l}{v}\right)^2 \frac{1}{\alpha_n^2}} \right]$$

where

$$\alpha_n^2 = \left((n+1)\frac{\pi}{2}\right)^2 \text{ and } \phi = \frac{wl}{v}$$

The impedance of the equivalent circuit in figure 4, assuming no resistive loss is :

$$Z = \frac{1}{j\omega(C_s + C_0)} \left[\frac{1 - \omega^2 L_s C_s}{1 - \omega^2 L_s \frac{C_s C_0}{C_s + C_0}} \right]$$

Equating the two expressions for the impedance yields the following :

$$C_0 = C \qquad C_s = \frac{C \frac{2K^2}{\alpha_n^2}}{1 - \frac{2K^2}{\alpha_n^2}} \qquad L_s = \frac{1}{C}\left(\frac{l}{v}\right)^2 \frac{1}{2K^2}$$

Bibliography

1. Thompson, P.A., *Design and performance of voltage controlled oscillators using TFR filters.* IEEE Frequency Control Symposium, 1989.
2. Cady, W.G., *Piezoelectricity.* 1946: Dover Publications Inc.
3. Lutsky, J., *Electrical Tuning of AlN Thin-Film Bulk Acoustic Resonators.*, in *Department of Electrical Engineering and Computer Science.* 1994, Massachusetts Institute of Technology.: Cambridge, MA.
4. Tsubouchi, K. *High frequency and low dispersion SAW devices for signal processing.* in *Ultrasonics Symposium.* 1980.
5. Dupuie, J.L., *Hot filament enhanced chemical vapor deposition of AlN thin films.* Applied Physics Letters, 1991. **59**(5): p. 549-551.
6. Saxler, A., *High quality aluminum nitride epitaxial layers grown on sapphire substrates.* Applied Physics Letters, 1994. **64**(3): p. 339-341.
7. Shiosaki, T. *Low temperature growth of piezoelectric AlN films by RF reactive magnetron sputtering.* in *IEEE Ultrasonics Symposium.* 1980.
8. Lakin, K. *Aluminum nitride thin film and composite bulk wave resonators.* in *IEEE Frequency Control Symposium.* 1982.
9. Ruby, R. *Micromachined thin film bulk acoustic resonators.* in *IEEE International Frequency Control Symposium.* 1994.
10. Kline, G. *Overmoded high Q resonators for microwave oscillators.* in *IEEE International Frequency Control.* 1993.
11. Rosenbaum, J., *Bulk Acoustic Wave Theory and Devices.* 1988: Artech House.
12. Kino, G., *Acoustic Waves.* 1987.
13. Chapman, B., *Glow Discharge Processes.* 1980: John Wiley and Sons.
14. Thornton, J. *Morphology of sputtered films.* in *Annual Review of Materials Science.* 1977.
15. Thompson, C. *Grain growth in thin films.* in *Annual Review of Materials Science.* 1990.
16. Ohuchi, F., *AlN thin films with controlled crystallographic orientations and their microstrucure.* Journal of Vacuum Science and Technology A, 1987. **5**(4): p. 1630-4.
17. Cullity, B., *Elements of X-ray Diffraction.* 1978: Addison Wesley.